A High-Resolution Model of the Planetary Boundary Layer—Sensitivity Tests and Comparisons with SESAME-79 Data

DALIN ZHANG

Department of Meteorology, The Pennsylvania State University, University Park 16802

RICHARD A. ANTHES

National Center for Atmospheric Research,[1] Boulder, CO 80307

(Manuscript received 30 April 82, in final form 23 July 1982)

ABSTRACT

A high-resolution, one-dimensional, moist planetary boundary layer (PBL) model is developed following Blackadar, and verified using the 10 April 1979 SESAME data set. The model consists of two modules to predict the time-dependent behavior of the PBL under various surface characteristics. Under stable conditions, turbulent fluxes are related to a local Richardson number. In contrast, under conditions of free convection, the exchange of heat, moisture and momentum occurs through mixing between convective elements originating at the surface and environmental air in the PBL.

Sensitivity tests showed that the daytime PBL structure is most sensitive to moisture availability, roughness length, albedo and thermal capacity, in that order. It is less sensitive in the nighttime to the above parameters. The wind profile is extremely sensitive to the specified geostrophic wind profile at all times. Simulations over both dry and moist terrain indicate that both the free convection (daytime) and the stable (nocturnal) modules are capable of accurately simulating the diurnal PBL evolution under nonsteady geostrophic conditions, provided accurate, time-dependent geostrophic wind profiles are available. With steady geostrophic forcing, the simulations are less realistic.

1. Introduction

It has been increasingly realized in recent years that the planetary boundary layer (PBL) is a critical factor in producing mesoscale weather systems such as convective storms, land–sea breezes, thermal boundaries and mountain–valley circulations (Pielke and Mahrer, 1975; Ogura and Chen, 1977; Ulanski and Garstang, 1978; McNider and Pielke, 1981; Pielke, 1981). Because of the large fluxes of heat, moisture and momentum that take place in this thin layer, there has been much interest in the incorporation of high-resolution PBL parameterizations into two- or three-dimensional mesoscale dynamical models. High-resolution, as opposed to mixed-layer models (e.g., Lilly, 1968; Lavoie, 1972) provide for more generality, for example, during the transition from well-mixed daytime conditions to stratified nocturnal conditions in which strong vertical gradients of temperature, wind and moisture often exist. Blackadar (1979) presents additional arguments for the need of high-resolution PBL models.

In this paper, we present a high-resolution, one-dimensional, moist PBL model following Blackadar (1976, 1978). To investigate the realism of the model in reproducing the behavior of the boundary layer in the real atmosphere before incorporation into a multi-dimensional model (Anthes and Warner, 1978), we will verify the one-dimensional version using the 10 April 1979 SESAME data set (Gerhard *et al.*, 1979). In addition, sensitivity tests will be conducted under steady geostrophic forcing to show the response of the model to different surface conditions.

The model tested here utilizes a first-order closure representation of turbulent effects under stable conditions, and a convective plume model under unstable conditions, and hence is considerably simpler and computationally more economic than second-order representations (see Mellor and Yamada, 1974, for a discussion of various higher-order representations). A number of other first-order schemes have been reported in the past, as reviewed by Blackadar (1979), Pielke (1981) and others. However, few of the previous studies include all of the following characteristics of this study, which are summarized in Table 1.

2. Description of the model

The PBL model contains two modules which represent two different regimes of turbulent mixing. One

[1] The National Center for Atmospheric Research is sponsored by the National Science Foundation.

0021-8952/82/111594-16$08.00

TABLE 1. Characteristics of the present study.

- Separate parameterizations for stable (nocturnal) and unstable (daytime) conditions are utilized
- A predictive slab model is used to obtain surface temperature
- Prognostic equations are utilized to calculate atmospheric variables in the surface layer
- Moisture is included in the coupled surface/PBL model
- Sensitivity tests to moisture availability, albedo, roughness and thermal capacity are presented
- 24 h simulations and predictions are presented, illustrating behavior of PBL under both day and night conditions
- Comparisons with observed data, available at 3 h intervals from the SESAME 1979 field program, are made
- A time-dependent geostrophic wind is utilized in real-data comparisons

is a nocturnal module in which K-theory is used; the value of K is determined by the local Richardson number. The second is a free-convection module which makes use of principles first proposed by Estoque (1968) and later developed by Blackadar (1976, 1978). The criterion that determines which module is operating is the magnitude of $|z_h/L|$ and the sign of the temperature gradient in the lowest model layers. Here z_h is the height of the mixed layer and L is the Monin-Obukhov length. The equations used in the model are

$$\frac{\partial \theta}{\partial t} = -\frac{1}{\rho}\frac{\overline{\partial \rho w'\theta'}}{\partial z}, \tag{1}$$

$$\frac{\partial q}{\partial t} = -\frac{1}{\rho}\frac{\overline{\partial \rho w'q'}}{\partial z}, \tag{2}$$

$$\frac{\partial u}{\partial t} = f(v - v_g) - \frac{1}{\rho}\frac{\partial}{\partial z}\overline{\rho u'w'}, \tag{3}$$

$$\frac{\partial v}{\partial t} = -f(u - u_g) - \frac{1}{\rho}\frac{\partial}{\partial z}\overline{\rho v'w'}, \tag{4}$$

where all the symbols assume their usual meteorological meaning, and fluctuations in density of air have been neglected. Phase changes of water and atmospheric radiation are assumed to occur only at the ground. Thus, the following description is devoted to how the ground variables and the flux terms for the nighttime and daytime modules are parameterized.

a. *Vertical structure of the model*

The vertical structure of the model is illustrated in Fig. 1. It consists of a substrate which represents a deep soil layer with invariant temperature, a slab which represents a thin layer of soil, a surface layer of fixed depth 10 m, and levels above with a vertical separation of 100 m.

All the prognostic variables (u, v, θ and q) are defined at the $z_{i+1/2}$ levels and all the diagnostic quantities, such as Richardson number Ri, the eddy exchange coefficient K, the fluxes of heat H, moisture Q, and momentum τ, are defined at z_i levels. For convenience, we use the subscript "a" to denote the surface layer and "g" for the ground.

b. *The ground parameterization*

In the sensitivity tests shown in the next section, it is apparent that the parameterization of the ground is the most important aspect determining the nature and behavior of the PBL. In the technique employed here, a slab model is utilized to compute the ground potential temperature θ_g through an energy budget equation

$$C_g\frac{\partial \theta_g}{\partial t} = R_n - H_m - H_g - E, \tag{5a}$$

where C_g is the thermal capacity of the slab per unit area (J m^{-2} °C^{-1}), H_m the heat flow into the substrate, H_g the heat flux into the atmosphere and E the latent heat flux. Blackadar (1979) shows that the following formulation enables the amplitude and phase of the slab temperature to be identical to the surface tem-

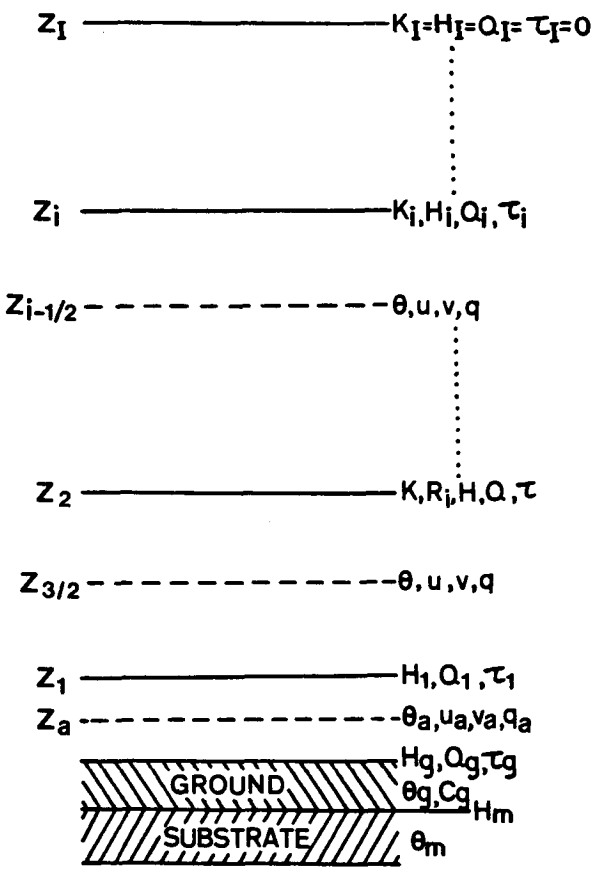

FIG. 1. Vertical structure of the PBL model.

perature of a real soil layer of uniform thermal conductivity λ and heat capacity per unit volume C_s, with C_g related to these parameters and the angular velocity of the earth ω by

$$C_g = 0.95\left(\frac{\lambda C_s}{2\omega}\right)^{1/2}. \tag{5b}$$

Deardorff (1978) found the performance of this slab technique to be superior to five other schemes in computing the ground temperature and heat flux. The essence of this treatment is that the sensible and latent heat fluxes (H_g and E) are partially compensated by fluxes of heat to and from a deep thermal reservoir.

The terms on the right-hand side (rhs) of (5a) are described as follows:

1) Radiative flux R_n

Radiation is the basic driving force of the diabatic PBL and the most important component of the slab energy budget. The amount of solar radiation absorbed by the slab is approximated as

$$Q_s = S(1 - A)(\cos\zeta)\tau_s^{\sec\zeta}, \tag{6}$$

where S denotes the intensity of solar radiation at the top of the atmosphere, A the albedo, ζ the solar zenith angle, τ_s the atmospheric transmissivity, and

$$\cos\zeta = \sin\psi \sin\delta + \cos\psi \cos\delta \cos h, \tag{7}$$

in which ψ represents the latitude of the location, δ the solar declination, and h the local hour angle of the sun (Sellers, 1974).

The net longwave radiation is divided into incoming $I\downarrow$ which is specified to be constant and outgoing $I\uparrow$ parts,

$$I\uparrow = \epsilon\sigma T_g^4, \tag{8}$$

where ϵ is the slab emissivity ($\sim$0.9–1.0), σ is the Stefan–Boltzman constant, and T_g the slab temperature which is obtained from the potential temperature. Hence, we can write

$$R_n = Q_s + I\downarrow - I\uparrow. \tag{9}$$

2) Heat flow into the substrate H_m

The transfer of heat due to molecular conduction is calculated from the equation

$$H_m = K_m C_g(T_g - T_m), \tag{10}$$

where K_m is the heat transfer coefficient expressed as $K_m = 1.18\omega$ and T_m is the temperature of the substrate (Blackadar, 1979).

3) Upward sensible heat flux H_g

The flux of sensible heat due to the combined molecular conduction and turbulent transfer is given as

$$H_g = K_s C_g(T_g - T_a), \tag{11}$$

in which the heat transfer coefficient K_s is made to be a function of the friction velocity such that $K_s = \omega + K_s' u^*$. A constant value of 3×10^{-3} m^{-1} is assumed for K_s'.

Table 2. Values of constants used in the model.

S	1370 J m^{-2} s^{-1}	K_0	1 m^2 s^{-1}
$I\downarrow$	275 J m^{-2} s^{-1}	K_s'	3×10^{-3} m^{-1}
τ_s	0.9	K_{qm}	2.4×10^{-5} m^2 s^{-1}
σ	5.6703×10^{-8} J m^{-2} K^{-4} s^{-1}	l	100 m
ω	7.27×10^{-5} s^{-1}		

4) The latent heat flux E

The latent heat flux is the most difficult component of the energy budget to model accurately. The moisture flux equation is of the form

$$Q_g = \overline{\rho w' q'} = -\rho K_q \frac{\partial q}{\partial z}. \tag{12}$$

Here, K_q denotes the transfer coefficient for moisture due to turbulent and molecular effects, where $K_q = K_{qt} + K_{qm}$. The K_{qm} is a constant background value (Table 2) which is included to permit slow diffusion when K_{qt} equals zero, and

$$K_{qt} = \frac{ku^* z}{\phi_h(z/L)}. \tag{13}$$

In (13), k is the Von Kármán constant and ϕ_h is the nondimensional temperature gradient that is a function of stability (Paulson, 1970). Solving for $\partial q/\partial z$ in (12) and integrating from the roughness length z_0 to z_a yields

$$q_a - q_g = -\frac{Q_g}{\rho}\int_{z_0}^{z_a}(K_{qm} + K_{qt})^{-1} dz. \tag{14}$$

In the general situation where $K_{qm}/K_{qt} \ll 1$ and with the replacement of the saturation specific humidity q_s for q_g, we obtain the approximate expression for latent heat flux

$$E = L_v Q_g = A_m \rho L_v\left(I_e^{-1} + \frac{K_{qm}}{z_a - z_0}\right)(q_s - q_a). \tag{15}$$

The quantity A_m is the moisture availability, a measure of the degree of saturation at the ground, and I_e is defined as

$$I_e = \int_{z_0}^{z_a} K_{qt}^{-1} dz. \tag{16a}$$

The integral of (16a) is well known (Paulson, 1970):

$$I_e = \frac{1}{ku^*}\left[\ln\frac{z_a}{z_0} - \psi_h(z_a/L)\right]. \tag{16b}$$

Expressions for $\psi_h(z_a/L)$ are given later in this paper.

The specification of moisture availability A_m is not straightforward because it is not easy to measure (Nappo, 1975). Carlson *et al.* (1981) formulated the moisture availability in terms of diurnal surface temperature difference, using satellite data and a boundary-layer model. However, here we specify it empirically, based on the 24 h changes of surface moisture and surface temperature.

c. *Nocturnal regime*

For the nocturnal module in which the atmospheric stratification is usually stable or at most marginally unstable, a first-order closure scheme is used. Here the eddy transfer coefficient K is a function of the Richardson number Ri. Since the largest gradients generally occur in the lowest layer, we define a 10 m surface layer in which Monin-Obukhov similarity is assumed to prevail (Webb, 1970; Businger and Arya, 1974).

1) THE SURFACE SCALING PARAMETERS

The nocturnal regime is subdivided into three categories which depend on the sign and magnitude of the bulk Richardson number Rb:

$$\mathrm{Rb} = \frac{gz_a}{\theta_a}\frac{(\theta_a - \theta_g)}{(V_a)^2}, \tag{17}$$

where V_a is the scalar wind speed at the surface.

For the case $\mathrm{Rb} \geqslant 0.2$, the surface layer is assumed to be so stable that no turbulence exists; thus, all fluxes, as well as the scaling parameters at the surface, such as H_1, Q_1, τ_1, z_a/L, ψ_h and ψ_m, are set equal to zero. When the condition $0.2 > \mathrm{Rb} > 0$ prevails, the surface layer is assumed to be in a state of damped mechanical turbulence. In this case, we compute the scaling parameters as follows:

$$\frac{z_a}{L} = \frac{\mathrm{Rb}}{1 - 5\,\mathrm{Rb}} \ln\frac{z_a}{z_0} \tag{18}$$

and

$$\psi_h = \psi_m = -5z_a/L. \tag{19}$$

The third situation, termed forced convection, is a marginally unstable state that occurs when $\mathrm{Rb} \leqslant 0$ and $|z_h/L| \leqslant 1.5$. The approximate formulas developed by Paulson (1970) and Blackadar (1976) can be used. Because an iteration procedure, which is time-consuming, is needed to solve for z_a/L, ψ_m, and ψ_h at each time step, we here treat the forced convection as a quasi-neutral case and the scaling parameters are approximately specified as

$$z_a/L = \mathrm{Ri}(z_1), \tag{20}$$

$$\psi_h = \psi_m = 0. \tag{21}$$

These approximations only slightly affected the results in numerous simulations.

Having obtained ψ_h and ψ_m from the damped mechanical turbulence regime or forced convection regime, we proceed to compute u^* for later use in the flux calculations

$$u^* = \frac{kV_a}{\ln(z_a/z_0) - \psi_m}. \tag{22}$$

Given u^*, the ground stress τ_g is calculated from

$$\tau_g = \rho u^{*2}, \tag{23}$$

and fluxes of sensible and latent heat can be obtained from (11) and (15).

2) PREDICTION OF THE SURFACE VARIABLES

In the present model, all variables in the surface layer are prognostic rather than diagnostic as in other PBL models:

$$\frac{\partial\theta_a}{\partial t} = [K_{h1}(\theta_{3/2} - \theta_a)/(z_{3/2} - z_a) + H_g/(\rho C_p)]/z_1, \tag{24}$$

$$\frac{\partial q_a}{\partial t} = [K_{q1}(q_{3/2} - q_a)/(z_{3/2} - z_a) + Q_g/\rho]/z_1, \tag{25}$$

$$\frac{\partial u_a}{\partial t} = [K_{m1}(u_{3/2} - u_a)/(z_{3/2} - z_a) - \tau_g u_a/(\rho V_a)]/z_1 + f(v_a - v_{ga}), \tag{26}$$

$$\frac{\partial v_a}{\partial t} = [K_{m1}(v_{3/2} - v_a)/(z_{3/2} - z_a) - \tau_g v_a/(\rho V_a)]/z_1 - f(u_a - u_{ga}). \tag{27}$$

The K-coefficient $K_m = K_h = K_q$ is determined by the Richardson number which is derived by Blackadar (1976) from second-order closure theory,

$$K_m = K_0 + S_i(kl)^2(\mathrm{Rc} - \mathrm{Ri})/\mathrm{Rc}. \tag{28}$$

K_0 is a background value, Rc the critical Richardson number, l a length that is presumed to characterize the turbulence containing energy, S_i the vertical wind shear, and Ri is the Richardson number defined as

$$\mathrm{Ri} = \frac{g}{\theta_a S_i^2}\frac{\theta_{i+1/2} - \theta_{i-1/2}}{z_{i+1/2} - z_{i-1/2}}. \tag{29}$$

A fixed value of 100 m is used for l and 0.25 for Rc. When the condition $\mathrm{Ri} > \mathrm{Rc}$ appears, the relatively strong temperature stratification suppresses the shear-generated turbulence so that the value of K_m is set equal to K_0.

3) PREDICTION OF VARIABLES ABOVE THE SURFACE

In all layers above the surface in the nocturnal regime, the prognostic variables are computed using K-theory, and an implicit diffusion scheme (Richtmyer,

1957) is utilized to calculate the turbulent terms. The eddy coefficients are provided by (28)–(29).

d. Free convection regime

Under strong solar heating, a super-adiabatic layer usually occurs in the lowest layer of the atmosphere. With their roots in the surface layer, buoyant plumes of hot air rise (Fig. 2). As these thermal elements ascend, mixing takes place at each level, thereby heating the environment and exchanging momentum and moisture. Some plumes overshoot into the overlying inversion. This penetration into the potentially warmer air results in a warming of the mixed layer and a growth and cooling of the inversion. Under these conditions, the vertical convective transfer of heat, moisture and momentum is not determined by local gradients, but by the thermal structure of the whole mixed layer and the surface heat flux. Hence, the vertical exchanges are visualized as taking place between the lowest layer and each level of the mixed layer, instead of between adjacent layers as in *K*-theory.

The intensity of mixing under free convection depends on the heat flux at the top of the surface layer. After analyzing a large number of measurements, Priestley (1956) derived an empirical equation for the heat flux H_1:

$$H_1 = \rho C_p z_1 b(\theta_a - \theta_{3/2})^{3/2}, \tag{30}$$

where b can be treated as a constant:

$$b = \left(\frac{2g}{27\theta_a}\right)^{1/2} \frac{1}{z_1}[z_1^{-1/3} - (2z_{3/2})^{-1/3}]^{-3/2}. \tag{31}$$

The potential temperature θ_a in the surface layer is obtained from

$$\frac{\partial \theta_a}{\partial t} = -(H_1 - H_g)/(\rho C_p z_1). \tag{32}$$

Above the surface, the rates of change of the prognostic variables are given by

$$\frac{\partial \theta_{i-1/2}}{\partial t} = \bar{m}(\theta_a - \theta_{i-1/2}), \tag{33}$$

$$\frac{\partial q_{i-1/2}}{\partial t} = \bar{m}(q_a - q_{i-1/2}), \tag{34}$$

$$\frac{\partial u_{i-1/2}}{\partial t} = \bar{m}(u_a - u_{i-1/2}) + f(v - v_g)_{i-1/2}, \tag{35}$$

$$\frac{\partial v_{i-1/2}}{\partial t} = \bar{m}(v_a - v_{i-1/2}) - f(u - u_g)_{i-1/2}, \tag{36}$$

in which $\bar{m}$ represents the fraction of mass exchange between any level and the surface layer per unit time. To determine the value of $\bar{m}$, the principle of heat energy conservation is used (Blackadar, 1978; Westphal, 1981) which leads to an expression for the heat flux at any level in the mixed layer of the form

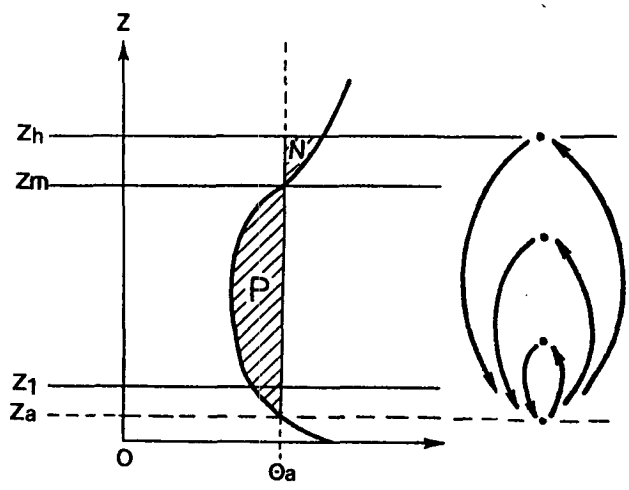

FIG. 2. Schematic diagram illustrating free convective module. Plumes originating at level z_a rise and mix at various levels, exchanging heat, moisture and momentum with air at these levels. Some thermals overshoot the level z_m of zero buoyancy. The ratio of negative area N on the thermodynamic diagram to the positive area P is the entrainment rate (see text).

$$H_i = H_1 - \bar{m}\rho C_p \int_{z_1}^{z_i} [\theta_a - \theta(z)]dz. \tag{37}$$

We assume no energy flux across the top of the mixed layer z_h, so that $H_i = 0$. Accordingly, (37) becomes

$$\bar{m} = H_1\left\{\rho C_p(1 - E_m)\int_{z_1}^{z_m} [\theta_a - \theta(z')]dz'\right\}^{-1}, \tag{38}$$

in which E_m denotes the fraction of the buoyant energy of a thermal element used for entrainment above the level z_m (see Fig. 2)

$$E_m = -\int_{z_m}^{z_h} [\theta_a - \theta(z)]dz \Big/ \int_{z_1}^{z_m} [\theta_a - \theta(z)]dz. \tag{39}$$

Theoretical and observational studies indicate that over homogeneous terrain, the downward heat flux due to entrainment is typically ~20% of the surface flux (Tennekes, 1975; Mahrt and Lenschow, 1976; Stull, 1976). Hence, the value of 0.2 is chosen for E_m, which is the ratio of negative area to positive area, as shown in Fig. 2. Knowledge of P and E_m enables z_h to be calculated (Fig. 2).

Given the value of $\bar{m}$, we can calculate the rate of change of the surface layer variables on the basis of conservation of momentum and moisture within the whole mixed layer. Specifically,

$$\frac{\partial u_a}{\partial t} = f(v_a - v_{ga}) - \left[\frac{\tau_g u_a}{\rho V_a} - \bar{m}\sum_{i=2}^{l}(u_a - u_{i-1/2})\Delta z\right] \Big/ z_1, \tag{40}$$

TABLE 3. The magnitude of surface parameters tested in the sensitivity studies.

	Low	Reference	High
Roughness z_0 (m)	0.01	0.1	1
Albedo A	0.1	0.2	0.3
Moisture availability A_m	0.0	0.1	0.5
Thermal capacity C_g (J m^{-2} K^{-1})	3×10^4	6×10^4	12×10^4

$$\frac{\partial v_a}{\partial t} = -f(u_a - u_{ga}) - \left[\frac{\tau_g v_a}{\rho V_a} - \bar{m}\sum_{i=2}^{l}(v_a - v_{i-1/2})\Delta z\right]\Big/ z_1, \quad (41)$$

$$\frac{\partial q_a}{\partial t} = [Q_g - \bar{m}\sum_{i=2}^{l}(q_a - q_{i-1/2})\Delta z]/(\rho z_1), \quad (42)$$

where the index l stands for the maximum height that the thermal reaches and all fluxes vanish.

To determine the stability regime at each new time step, the stability parameters are computed from the most recent value of the temperature, heat flux, and friction velocity according to

$$\frac{1}{L} = -\frac{kgH_1}{C_p\rho\theta_a u^{*3}}. \quad (43)$$

To increase the speed of the model, the Paulson relations for ψ_m and ψ_h are approximated by polynomials

$$\psi_m = 0.0954 - 1.86(z_a/L) - 1.07(z_a/L)^2 - 0.249\left(\frac{z_a}{L}\right)^3, \quad (44)$$

$$\psi_h = 0.201 - 3.23(z_a/L) - 1.99\left(\frac{z_a}{L}\right)^2 - 0.474\left(\frac{z_a}{L}\right)^3. \quad (45)$$

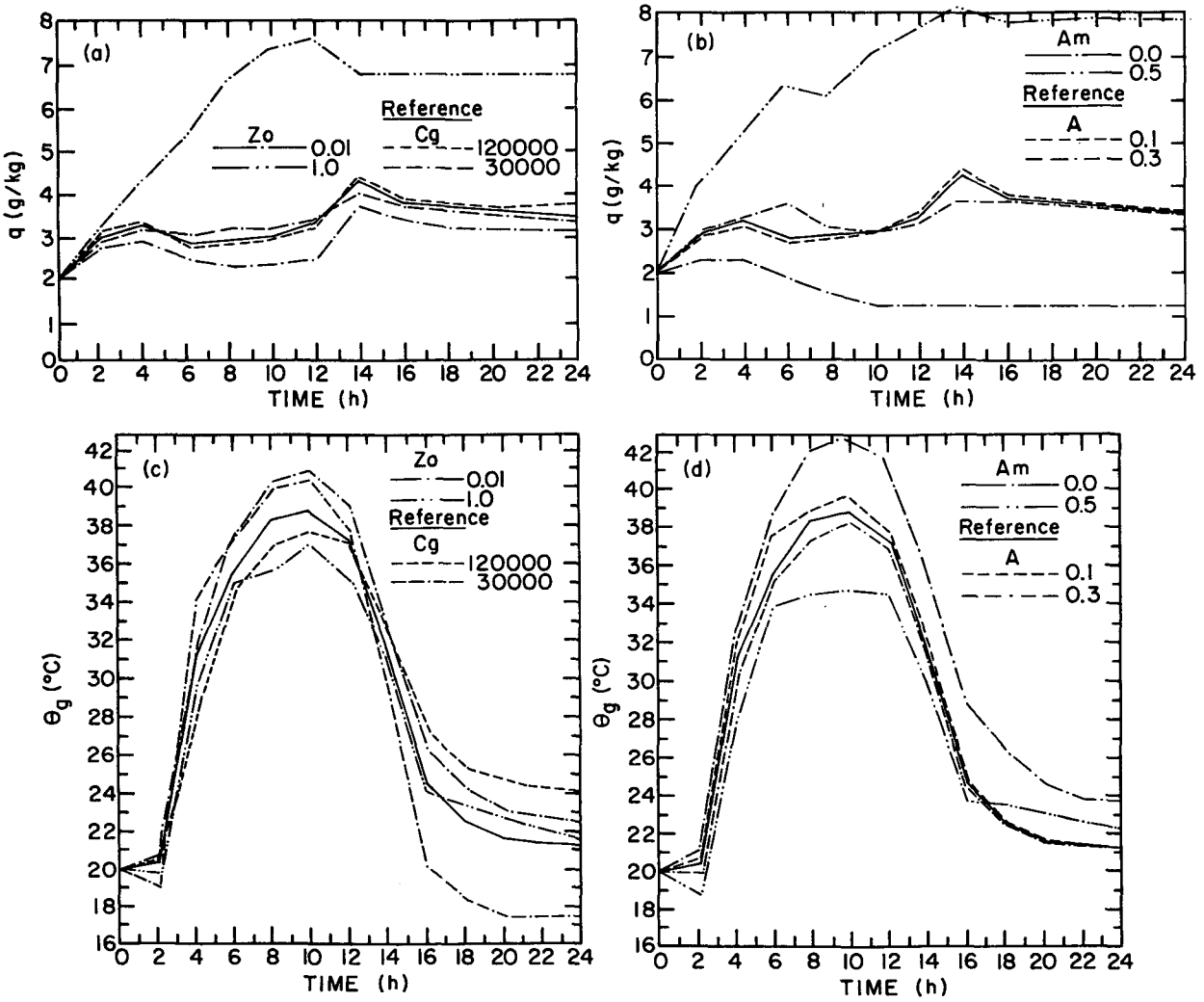

FIG. 3. Temporal variation of surface layer specific humidity q and ground potential temperature θ_g for sensitivity experiments in which roughness parameter z_0, thermal capacity C_g, moisture availability A_m, and albedo A are varied. See text for details.

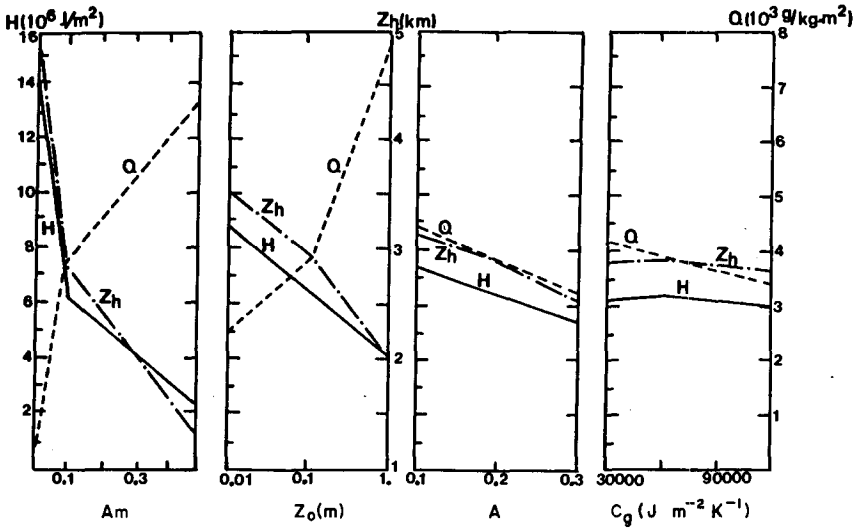

FIG. 4. 12 h vertical integrals of sensible heat flux H, water vapor flux Q, and height of mixed layer z_h for three values of moisture availability A_m, roughness parameter z_0, albedo A, and thermal capacity C_g.

In (44) and (45), a lower limit of -2 is set for z_a/L. The friction velocity u^* is computed from (22). For the tendencies of variables above the convective domain, the nocturnal module is used and the implicit scheme is utilized for the eddy flux term.

e. *Computational procedures*

All model constants are given in Table 2. The difference $\theta_g - \theta_a$ and the stability parameter z_h/L are checked every time step, to determine which module is applicable. Then the friction velocity u^* is used to calculate H_g, Q_g and τ_g, and θ_a, q_a, u_a and v_a are computed from (24)–(27) in the nocturnal mode or from (32) and (40)–(42) in the free convection regime.

To minimize the computational mode, a small time step at the beginning of the integration is utilized, which then increases until the regular time-increment of 30 s is reached. In addition, a time-filter is utilized to avoid the separation of solutions (Asselin, 1972). The small value of Δt is chosen for maximum accuracy; it is not necessary for computational stability. The model is stable for values of Δt at least as large as 150 s.

Because a small vertical increment (Δz = 10 m) is used for the surface layer, a number of short time steps are required to compute the variables in the atmospheric surface layer for every long time step used for the other layers. Details may be found in Westphal (1981) and Zhang (1981).

3. Sensitivity of the model to the specified parameters

To determine the relative significance of some key parameters in determining the vertical profiles of potential temperature, moisture and wind velocity, sensitivity tests of the model to the roughness z_0, albedo A, moisture availability A_m, and thermal capacity of the slab C_g are conducted. A reference state is defined from which the parameters are systematically varied (Table 3).

The model was initialized with data from Marfa, TX (SESAME-1) at 0400 LST 10 April 1979 (Fig. 9) and integrated for 24 h assuming a steady geostrophic wind. The results from the sensitivity experiments are shown in Figs. 3–5. Fig. 3 shows the temporal variation of surface humidity and ground potential temperature. Fig. 4 shows the height of the PBL and the vertical integrals of sensible heat and water vapor after 12 h of integration (the end of the heating cycle), and Fig. 5 shows the vertical profiles of potential temperature, specific humidity and wind speed at 12 h and 24 h. The profiles of temperature and moisture above 500 m change only slightly after 12 h, and therefore are not shown.

a. *Significance of moisture availability*

Variations in moisture availability A_m cause large differences in the model variables, especially when A_m is less than the reference value. As shown in Fig. 3b, the surface moisture varies from <2 g kg^{-1} at 12 h for $A_m = 0$, to over 8 g kg^{-1} when $A_m = 0.5$. As A_m increases, θ_g decreases (Fig. 3d), since more of the incoming solar radiation is used in evaporation. The vertical integrals of sensible and latent heat and the maximum height of the PBL also show a strong dependence on A_m (Fig. 4).

The vertical profiles of θ, q and wind speed (Fig. 5) indicate a cooler, moister boundary layer of decreasing depth as A_m is increased. The wind speed profiles show the greatest effect at 12 h, after the com-

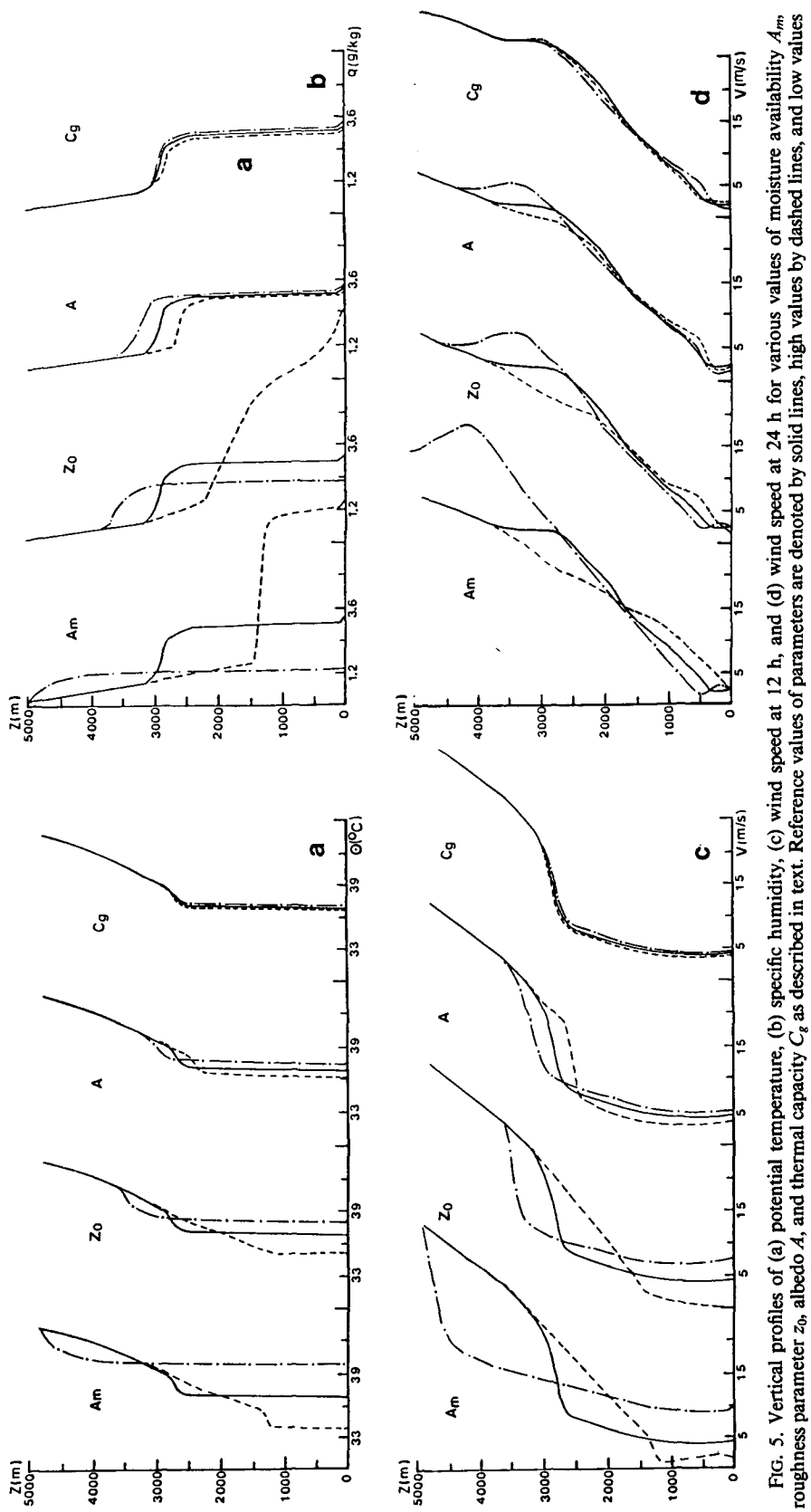

FIG. 5. Vertical profiles of (a) potential temperature, (b) specific humidity, (c) wind speed at 12 h, and (d) wind speed at 24 h for various values of moisture availability A_m, roughness parameter z_0, albedo A, and thermal capacity C_g as described in text. Reference values of parameters are denoted by solid lines, high values by dashed lines, and low values by dash-dot lines (see Table 3).

pletion of the heating cycle, with stronger winds in the PBL occurring with $A_m = 0$. These differences indicate that small changes in moisture availability will probably make significant changes in the boundary layer of three-dimensional models, and its specification should be done with care.

b. *Significance of roughness length*

The effect of increasing the roughness length is to increase the frictional drag, mixing and evaporation. The heat flux is reduced due to the stronger evaporation. Because of the increased friction and evaporational cooling for high z_0, a decrease in momentum and temperature occurred in the surface layer. The wind speed was reduced by 7 m s^{-1} and the temperature by 4°C, compared to the simulation with low z_0. The increased evaporation and reduced depth of the PBL associated with a high z_0 permit the low-level moisture to accumulate to high values (Figs. 3a and 5b). Thus, the PBL structure is quite sensitive to an order of magnitude change in z_0.

c. *Significance of thermal capacity*

The response of the model during the daytime to variations in the thermal capacity is relatively weak. Within the range of a factor of four change in C_g, there was less than 10% variation in the height of the mixed layer, the ground temperature, and total heat and moisture content of the mixed layer (Figs. 3 and 4). The sensitivity of the vertical profiles is also small (Fig. 5). The reason for this small sensitivity is that the surface heat budget during the day is dominated by evaporation for the reference value of A_m, and the soils with different thermal capacities evaporated moisture at nearly the potential rate. However, reducing the magnitude of C_g, increased the ground temperature by 3.5°C at the time of strong sunshine and increased the ground cooling by 7°C (Fig. 3c) when infrared radiation dominated and the latent heat effect was negligible.

TABLE 4. Specification of surface variables for case studies.

	MLU	MRF
A_m	0.2	0.04
z_0 (m)	0.1	0.1
A	0.18	0.1
C_g (J m^{-2} K^{-1})	12×10^4	3×10^4
θ_m (K)	294.5	301.0
ϵ	0.95	1.0
θ_{g0} (K)	284.8	293.2
P_{g0} (mb)	1005	840
ψ (deg)	32.5	30.2
λ (deg longitude)	92	104

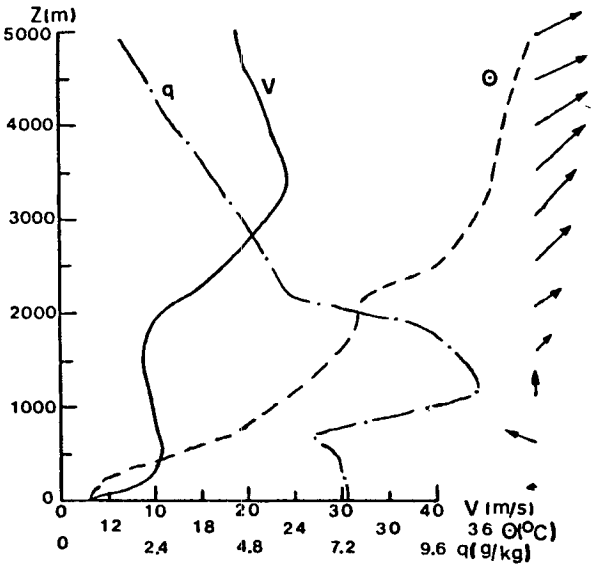

FIG. 6. Initial vertical profiles of potential temperature θ, specific humidity q, and wind speed V for model simulations at Monroe, 1200 GMT 10 April 1979.

d. *Significance of albedo A*

A smaller albedo implies a larger fraction of incoming radiation which can be absorbed by the ground and an increase in the heat-driven turbulence. The resulting high ground temperature and strong turbulent transfer promoted stronger surface evaporation, which acted to reduce the amount of the temperature increase. The net result was a linear response to variations in the magnitude of A (Fig. 4). The maximum differences of the mixed-layer temperature, wind speed and moisture are approximately 1.5°C, 2 m s^{-1}, and 0.2 g kg^{-1}, respectively.

e. *Summary of sensitivity tests*

In the above tests, all profiles were symmetrically distributed on both sides of the reference curves, i.e., the response was approximately linear over the range of variation tested. For the experiments here, the moisture availability produced the largest model response, and thus is of critical importance in determining the daytime structure of the mixed layer. This result agrees with that of McCumber and Pielke (1981). Second to moisture availability, the roughness length was an important factor in producing the low-level behavior of the wind and the energy budget. The large changes in albedo tested here, somewhat affected the response of the model, but smaller changes would likely have little effect. The variation in thermal capacity of the slab produced the least influence on the solutions during the daytime when evaporation dominated the heat budget, but had an appreciable effect on the low-level structure after sunset.

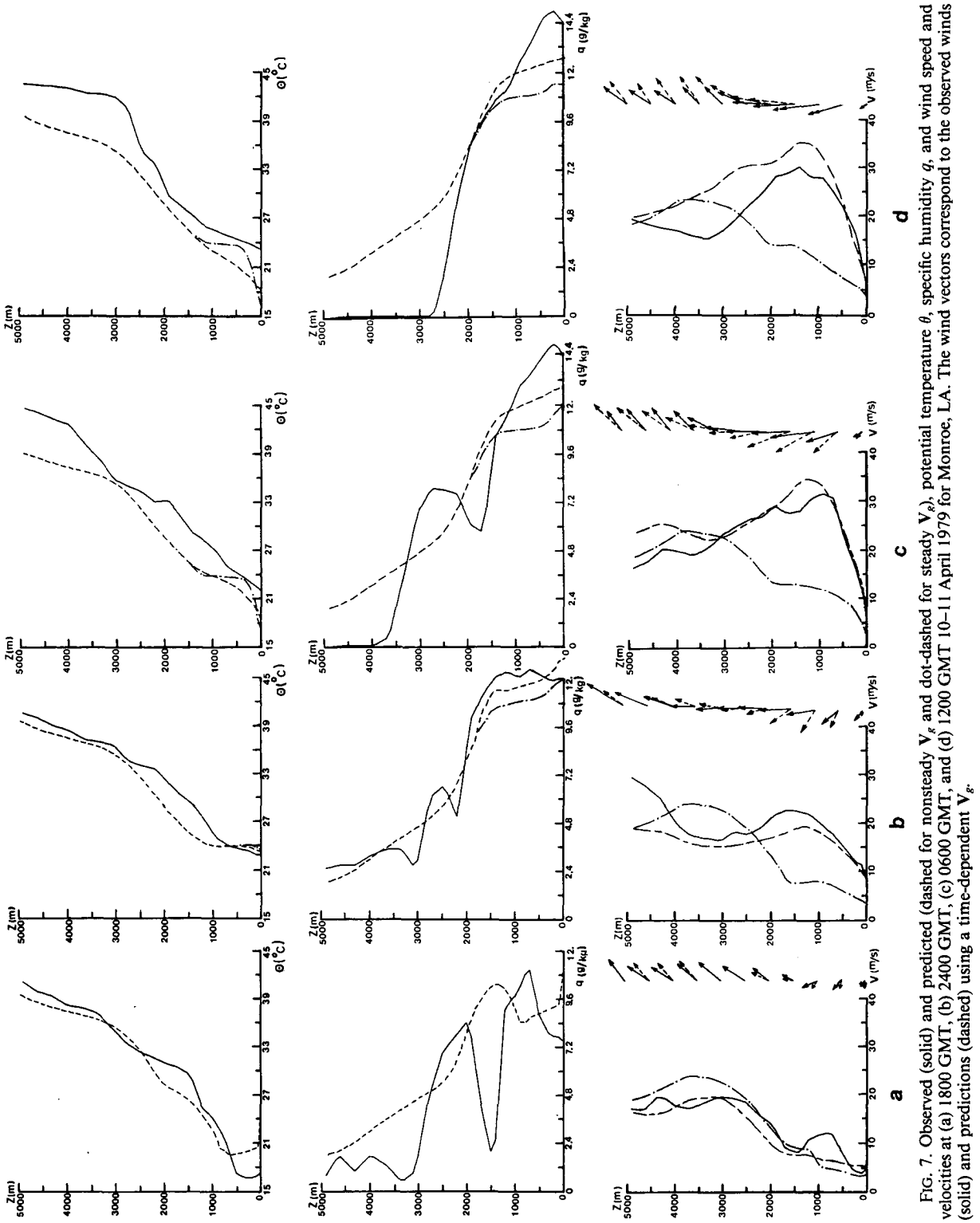

FIG. 7. Observed (solid) and predicted (dashed for nonsteady $\mathbf{V}_g$ and dot-dashed for steady $\mathbf{V}_g$), potential temperature θ, specific humidity q, and wind speed and velocities at (a) 1800 GMT, (b) 2400 GMT, (c) 0600 GMT, and (d) 1200 GMT 10–11 April 1979 for Monroe, LA. The wind vectors correspond to the observed winds (solid) and predictions (dashed) using a time-dependent $\mathbf{V}_g$.

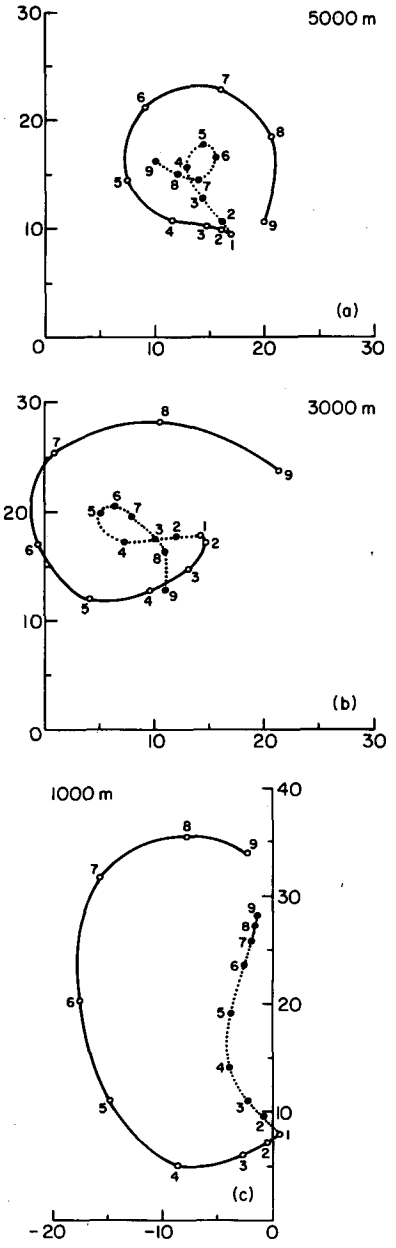

FIG. 8. Hodographs of observed geostrophic wind (dotted curves) and model-predicted winds (solid curves) at 5000, 3000 and 1000 m for Monroe, LA. Points are numbered at 3-h intervals beginning with 1200 GMT 10 April 1979.

The sensitivity of the profiles above the surface during the night to variations in the surface parameters is small, since the nocturnal PBL decouples from the surface shortly after sunset. After sunset, the ground affects only the lowest 200–500 m layer. However, variations in the surface forcing during daytime affected considerably the later development of the wind profile, specifically, the strength and location of the nocturnal jet (Fig. 5d).

With these results, we may state that the following meteorological conditions tend to be favorable for the development of strong PBL convective turbulence:

- small moisture availability,
- aerodynamically smooth surface with $A_m \neq 0$,
- rough land with $A_m = 0$,
- small albedo,
- small thermal capacity of the soil.

4. Comparison with observations

a. Data and initialization

To compare the model predictions with observations, two data sets were selected from the SESAME-1979 experiments. This experiment included 3 h rawinsonde soundings at 23 National Weather Service stations plus 16 supplemental sites with 25 mb vertical resolution from anemometer level to the 25 mb level. Hence, the desired time and vertical resolution for the PBL modeling were obtained. The synoptic aspects of this case are presented by Carlson *et al.* (1980) and Anthes *et al.* (1982).

Because of the one-dimensional nature of the PBL model and some limitations of the model physics (such as the neglect of clouds), data sets had to be carefully selected from the 39 upper-air stations. The primary criteria in selecting data were that the influences of extensive cloud cover and precipitation be excluded. It was also necessary to consider only stations with nearly complete data sets for the time period. Accordingly, stations Monroe, LA (MLU) and Marfa, TX (MRF) were chosen to test the model.

Unfortunately, the SESAME-1 experiment did not provide the necessary surface parameters. To give as realistic values as possible for z_0, A, C_g and A_m, the parameters for each location were determined from the *National Atlas of the United States of America* (Gerlach, 1970) in combination with knowledge from the sensitivity tests. The information includes characteristics of land use, vegetation and soil. The potential temperature of the substrate θ_m was obtained by averaging the surface potential temperature over the 24 h period. The values of all these parameters for the two case studies are given in Table 4.

The accurate specification of the vertical profile of the geostrophic wind is extremely important in determining the evolution of the wind profile, especially in this one-dimensional model in which mutual adjustments between the wind and mass field cannot occur (Zhang, 1981). The time-dependent vertical profiles of $\mathbf{V}_g$ were determined as follows. First, the geopotential data were analyzed every 3 h on the constant pressure surfaces provided by the SESAME data set (25 mb resolution) and the geostrophic winds computed at each level by a box method described by Forbes *et al.* (1982). Then values of $\mathbf{V}_g$ every 3 h were determined at the model levels by linear interpolation. After smoothing the profiles in time, profiles

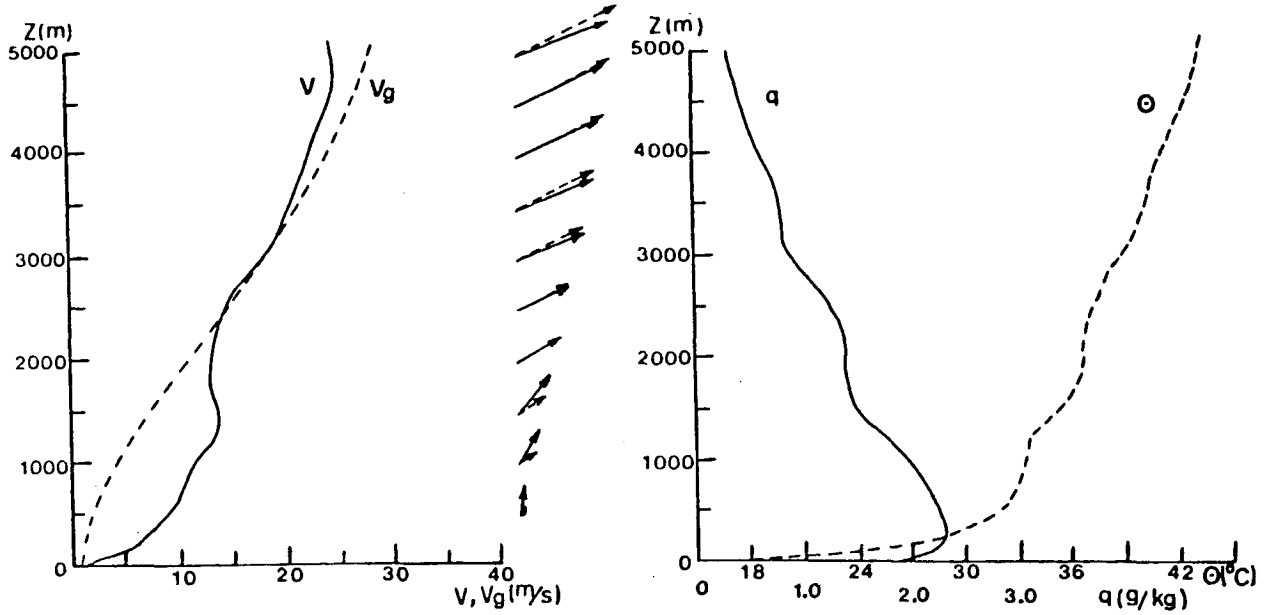

FIG. 9. Initial vertical profiles of potential temperature θ, specific humidity q, wind speed V, and geostrophic wind speed $\mathbf{V}_g$ for Marfa, TX, 1200 GMT 10 April 1979.

of $\mathbf{V}_g$ at every model time step were obtained by interpolation. During the integration, the interpolated values of $\mathbf{V}_g$ were used in the prognostic equation for u and v in the PBL. Above the PBL, the observed winds were used as estimates for $\mathbf{V}_g$, under the assumption that above the PBL, where the flow is quasi-geostrophic, the observed winds are a better measure of the geostrophic winds than could be obtained from the geopotential data on this scale.

b. Predictions

Two forecasts were made beginning at 1200 GMT 10 April 1979. Comparisons of the observed structure of the potential temperature, specific humidity, and wind velocity with their predicted profiles up to a level of 5 km will be given every 6 h. To illustrate the importance of $\mathbf{V}_g$, predictions are made with both steady (equal to the initial) and time-dependent profiles of $\mathbf{V}_g$.

1) A SIMULATION OVER A MOIST SURFACE (MONROE, LA)

Monroe, LA (MLU) was considered a location with a moist surface, and A_m was set equal to 0.2. On 10 April 1979, the synoptic conditions were nearly steady and advection effects were small until a warm front approached at 0000 GMT 11 April. Satellite imagery indicated clear skies during most of the period.

Initial profiles are shown in Fig. 6 and comparisons of the predicted and observed profiles are displayed in Fig. 7. The temperature profiles show considerable warming below 1000 m during the first 6 h (compare Figs. 6 and 7a), with the model predicting somewhat higher values of θ than were observed. By 12 h, the agreement in the lowest kilometer is quite close (Fig. 7b). During the daytime portion of the forecast, the specific humidity also increases, from an initial surface value of ~ 7 g kg^{-1} to ~ 12 g kg^{-1} at 2400 GMT. This increase was forecast well by the model (Fig. 7b). The wind profiles at 1800 and 2400 GMT (Fig. 7a, b) show the importance of a time-dependent geostrophic wind; the solution with a steady $\mathbf{V}_g$ is far inferior to the solution with variable $\mathbf{V}_g$.

During the development of the nocturnal PBL, the forecasts tended to gradually depart from the observations, due to the fact that synoptic influences became important. However, under the time-dependent geostrophic conditions, the model yielded a reasonable moisture prediction at 24 h in the lower layers with a 2 g kg^{-1} underestimate, because of an excessive cooling of ~ 5°C (see Fig. 7d). Meanwhile, the low-level winds were well-predicted, including the development of the south-southeasterly low-level "jet." As proposed by Blackadar (1957), this jet was produced after sunset when the atmosphere above 1 km became decoupled from the surface.

To better understand the response of the wind at different levels to the time-dependent geostrophic flow, hodographs of predicted and geostrophic velocities at 1000, 3000 and 5000 m are given in Fig. 8. Under the time-dependent geostrophic flow, the winds at higher levels undergo an oscillation which lags behind the geostrophic flow. At lower levels, an

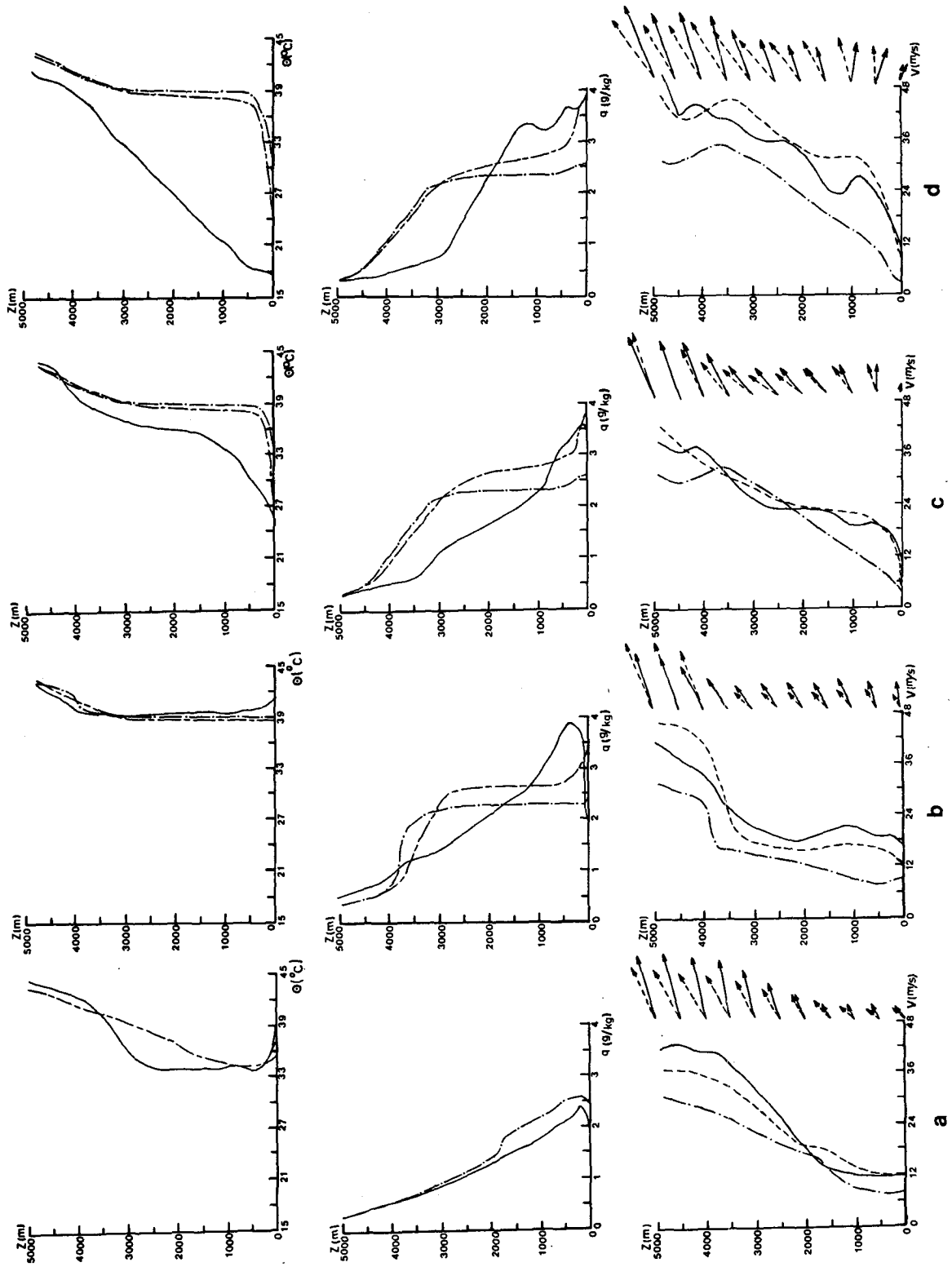

FIG. 10. Observed (solid) and predicted (dashed for time-dependent $\mathbf{V}_g$ and dot-dashed for steady $\mathbf{V}_g$) profiles of potential temperature θ, specific humidity q, wind speeds and velocities at (a) 1800 GMT, (b) 2400 GMT, (c) 0600 GMT, and (d) 1200 GMT 10–11 April 1979 for Marfa, TX. The wind vectors correspond to the observed winds (solid) and predictions (dashed) using a time-dependent $\mathbf{V}_g$.

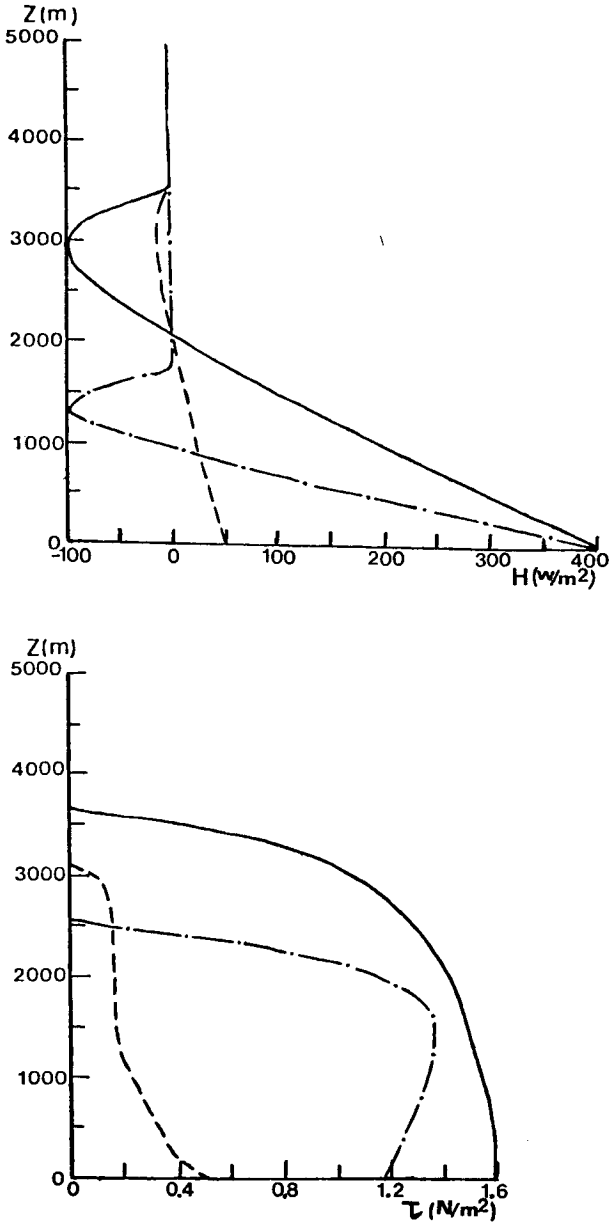

FIG. 11. Model-predicted vertical profiles of heat flux H and stress τ at 1800 GMT (dash-dot), 2100 GMT (solid) and 2400 GMT (dashed) for Marfa, TX, 10 April 1979.

intensifying pressure gradient force increased the predicted winds. The ageostrophic component of the flow may be somewhat unrealistic, since there is no feedback of the wind changes to the specified pressure changes, which prevents a correct geostrophic adjustment.

2) A SIMULATION OVER A DRY SURFACE (MARFA, TX)

The weather at Marfa, TX (MRF) on 10 April 1979 was clear and dry with southwesterly winds in advance of a cold front, which reached MRF shortly after sunset. Initial profiles of potential temperature, moisture, and wind velocity are presented in Fig. 9.

The predictions are compared with observations in Fig. 10. The structure of the mixed layer during the daytime was reasonably well modeled. The potential temperature profiles show rapid warming while the specific humidity profiles show little change (in comparison with the previous moist prediction). As in the previous case, the model wind profiles agree most closely with the observed profile when the time-dependent geostrophic wind profile is utilized.

After sunset, as the cold front passed, cold advec-

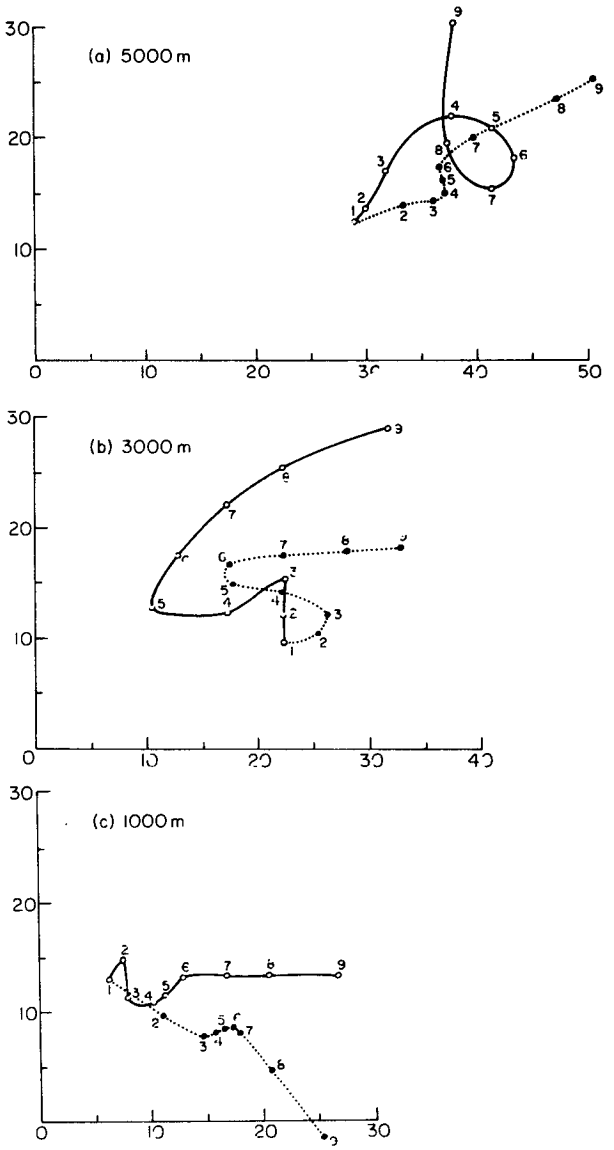

FIG. 12. Hodographs of observed geostrophic wind (dotted curves) and model-predicted winds (solid curves) at 5000, 3000 and 1000 m for Marfa, TX.

tion led to a progressive decrease in temperature at the lower layers in addition to the radiational cooling. Hence, large errors in the predicted temperature occurred (Fig. 10c, d).

The agreement between the predicted and observed specific humidity was fair on the whole, and best in lower layers, again with time-dependent geostrophic forcing. Higher up, the effect of dry advection produced a larger error near the top of the mixed layer.

The model-predicted winds with the nonsteady $\mathbf{V}_g$ showed good agreement at all levels and all times. During the early development of the mixed layer (1200 to 1800 GMT), vigorous convective eddies produced a momentum convergence below 1 km, which accelerated the wind (see Figs. 10 and 11). In the late afternoon, these eddies tended to dissipate, as indicated by the momentum divergence at 2100 and 2400 GMT (Fig. 11).

The hodographs (Fig. 12) indicate that the geostrophic wind increased at all levels during the simulation period. In response, the predicted winds and ageostrophic motion also increased. This behavior is consistent with Mahrt's (1974) conclusion from an analytic solution that an intensifying geostrophic flow is favorable for the development of ageostrophic motion, if there is no mutual adjustment mechanism.

5. Summary and conclusions

In this paper, a modified version of Blackadar's (1976, 1978) model was verified using 24 h data from the SESAME 10 April 1979 experiment. In addition, sensitivity tests showed that the PBL, primarily the buoyancy-driven mixed layer, is highly sensitive to surface characteristics. When these surface characteristics were appropriately specified, the one-dimensional model was fairly successful in simulating atmospheric structure under time-dependent geostrophic wind conditions, provided that the geostrophic wind profiles were realistically specified. The forecast and observed profiles of potential temperature, moisture and winds in the mixed layer were closely correlated during the daytime. Although there were large departures in the forecast nocturnal thermal structure from the observations, the nocturnal module still provided reasonable simulations of nighttime turbulence episodes, in view of the neglect of radiation and large-scale horizontal and vertical advection. Because of the neglect of these effects, the forecast nocturnal inversion could develop only to a depth of 300–600 m.

The model was very sensitive to variations in the geostrophic flow. An intensifying pressure gradient resulted in an increase in both predicted wind speed and the ageostrophic motion, since there was no mutual adjustment mechanism in the model. However, the model was accurate in duplicating the wind profile at all levels and all times when accurate geostrophic conditions were prescribed.

Refinement of this PBL model could be envisaged in various directions. One physical improvement would be to incorporate infrared radiation into the nocturnal module, since the development of the nocturnal PBL is determined by both radiative transfer and turbulence. Other improvements would be the representation of clouds and vegetation in the model.

Finally, we emphasize that a one-dimensional planetary boundary layer is greatly limited by the requirement for a specified, time-dependent geostrophic wind profile and the neglect of horizontal and vertical advection. However, the present model is an economical and efficient tool for isolating effects of the surface and vertical mixing. We conclude that the one-dimensional model proposed in this paper, if incorporated into a multi-dimensional dynamic model, is capable of simulating atmospheric flows in the PBL, because the latter can provide the effects of advection and changing horizontal pressure gradient and the necessary mutual adjustment mechanisms.

Acknowledgments. We thank Dr. Thomas Warner for his review and assistance, and Mr. Daniel Baldwin for his discussions. Robert Dickinson provided a thorough review of the manuscript. The first author expresses his sincere appreciation to the Academy of Science of China for financial support (scholarship) during the preparation of this work. This research was conducted under contract NSG-5205. The computations were performed using PDP-11 of the Department of Meteorology at the Pennsylvania State University. Ann Modahl at the National Center for Atmospheric Research provided editorial and typing assistance.

REFERENCES

Anthes, R. A., and T. T. Warner, 1978: Development of hydrodynamic models suitable for air pollution and other mesometeorological studies. *Mon. Wea. Rev.*, **106,** 1045–1078.

——, Y-H. Kuo, S. G. Benjamin and Y-F. Li, 1982: The evolution of the mesoscale environment of severe local storms: Preliminary modeling results. *Mon. Wea. Rev.*, **110,** 1187–1213.

Asselin, R., 1972: Frequency filter for time integrations. *Mon. Wea. Rev.*, **100,** 487–490.

Blackadar, A. K., 1957: Boundary layer wind maxima and their significance for the growth of nocturnal inversions. *Bull. Amer. Meteor. Soc.*, **38,** 283–290.

——, 1976: Modeling the nocturnal boundary layer. *Preprints, Third Symp. on Atmospheric Turbulence, Diffusion and Air Quality*, Raleigh, Amer. Meteor. Soc., 46–49.

——, 1978: Modeling pollutant transfer during daytime convection. *Preprints, Fourth Symp. on Atmospheric Turbulence, Diffusion, and Air Quality*, Reno, Amer. Meteor. Soc., 443–447.

——, 1979: High resolution models of the planetary boundary layer. *Advances in Environmental Science and Engineering*, Vol. 1, No. 1, J. Pfafflin and E. Ziegler, Eds., Gordon and Breach, 50–85.

Businger, J. A., and S. P. S. Arya, 1974: Height of the mixed layer in the stably stratified planetary boundary layer. *Advances in Geophysics*, Vol. 18A, Academic Press, 73–92.

Carlson, T. N., J. K. Dodd, S. G. Benjamin and J. N. Cooper, 1981: Satellite estimation of the surface energy balance, mois-

ture availability and thermal inertia. *J. Appl. Meteor.*, **20,** 67–87.

——, R. A. Anthes, M. Schwartz, S. G. Benjamin and D. G. Baldwin, 1980: Analysis and prediction of severe storms environment. *Bull. Amer. Meteor. Soc.*, **61,** 1018–1032.

Deardorff, J. W., 1978: Efficient prediction of ground surface temperature and moisture with inclusion of a layer of vegetation. *J. Geophys. Res.*, **83,** 1889–1903.

Estoque, M. A., 1968: Vertical mixing due to penetrative convection. *J. Atmos. Sci.*, **25,** 1046–1051.

Forbes, G. S., R. A. Anthes and D. W. Thomson, 1982: Synoptic and mesoscale aspects of an Appalachian ice storm. Submitted to *Mon. Wea. Rev.*

Gerhard, M. L., H. E. Fuelberg, S. F. Williams and R. E. Turner, 1979: AVE-SESAME 1: 25-mb sounding data. NASA TM-78256, Marshall Space Flight Center, AL, 364 pp.

Gerlach, A. C., Ed., 1970: *The National Atlas of the United States of America.* U.S. Dept. Interior, Geological Survey, Washington, DC, 417 pp.

Lavoie, R. L., 1972: A mesoscale numerical model of lake-effect storms. *J. Atmos. Sci.*, **29,** 1025–1040.

Lilly, D. K., 1968: Models of cloud-topped mixed layers under a strong inversion. *Quart. J. Roy. Meteor. Soc.*, **94,** 292–309.

Mahrt, L. J., 1974: Time-dependent, integrated planetary boundary layer flow. *J. Atmos. Sci.*, **31,** 457–464.

——, and D. H. Lenschow, 1976: Growth dynamics of the convectively mixed layer. *J. Atmos. Sci.*, **33,** 41–51.

McCumber, M. C., and R. A. Pielke, 1981: Simulation of the effects of surface fluxes of heat and moisture in a mesoscale numerical model. 1. Soil layer. *J. Geophys. Res.*, **86,** 9929–9938.

McNider, R. T., and R. A. Pielke, 1981: Diurnal boundary-layer development over sloping terrain. *J. Atmos. Sci.*, **38,** 2198–2212.

Mellor, G. L., and T. Yamada, 1974: A hierarchy of turbulence closure models for planetary boundary layers. *J. Atmos. Sci.*, **31,** 1791–1806.

Nappo, C. J., 1975: Parameterization of surface moisture and evaporation rate in a planetary boundary layer model. *J. Appl. Meteor.*, **14,** 289–296.

Ogura, Y., and Y. L. Chen, 1977: A life history of an intense mesoscale convective storm in Oklahoma. *J. Atmos. Sci.*, **34,** 1458–1476.

Paulson, C. A., 1970: The mathematical representation of wind speed and temperature profiles in the unstable atmospheric surface layer. *J. Appl. Meteor.*, **9,** 857–861.

Pielke, R. A., 1981: Mesoscale numerical modeling. *Advances in Geophysics*, Vol. 23. Academic Press, 185–344.

——, and Y. Mahrer, 1975: Representation of the heated planetary boundary layer in mesoscale models with coarse vertical resolution. *J. Atmos. Sci.*, **32,** 2288–2308.

Priestley, C. H. B., 1956: Convection from the earth's surface. *Proc. Roy. Soc. London*, **A238,** 287–304.

Richtmyer, R. D., 1957: *Difference Methods for Initial-Value Problems.* Interscience, 283 pp.

Sellers, W. D., 1974: *Physical Climatology.* University of Chicago Press, 272 pp.

Stull, R. B., 1976: Mixed-layer depth model based on turbulent energetics. *J. Atmos. Sci.*, **33,** 1268–1278.

Tennekes, H., 1975: Reply. *J. Atmos. Sci.*, **32,** 992–995.

Ulanski, S. L., and M. Garstang, 1978: Role of surface divergence and vorticity in the life cycle of convective rainfall. Part I: Observation and analysis. *J. Atmos. Sci.*, **36,** 1047–1062.

Webb, E. K., 1970: Profile relationships: The log-linear range and extension to strong stability. *Quart. J. Roy. Meteor. Soc.*, **96,** 67–90.

Westphal, D. L., 1981: The interaction between radiative and boundary layer processes in stratus clouds. M.S. thesis, The Pennsylvania State University, 138 pp.

Zhang, D. L., 1981: A verification of one-dimensional model simulations of the planetary boundary layer over dry and moist terrain. M.S. thesis, The Pennsylvania State University, 91 pp.